Transport of Neutrally Buoyant and Dense Variably Sized Colloids in a Two-Dimensional Fracture with Anisotropic Aperture

ARTICLE *in* TRANSPORT IN POROUS MEDIA · JANUARY 2003

Impact Factor: 1.55 · DOI: 10.1023/A:1021952226861

2 AUTHORS:

Constantinos V. Chrysikopoulos
Technical University of Crete
143 PUBLICATIONS **1,990** CITATIONS
SEE PROFILE

Scott C James
Baylor University
118 PUBLICATIONS **579** CITATIONS
SEE PROFILE

Transport in Porous Media **51:** 191–210, 2003.

Transport of Neutrally Buoyant and Dense Variably Sized Colloids in a Two-Dimensional Fracture with Anisotropic Aperture

CONSTANTINOS V. CHRYSIKOPOULOS[1] and SCOTT C. JAMES[2]
[1]*Department of Civil and Environmental Engineering, University of California, Irvine, CA 92697-2175, USA. e-mail: costas@eng.uci.edu*
[2]*Performance Assessment and Decision Analysis Department, Sandia National Laboratories, Carlsbad, NM 88220, USA. e-mail: scjames@sandia.gov*

(Received: 10 December 2001; in final form: 1 May 2002)

Abstract. The transport of monodisperse as well as polydisperse colloid suspensions in a two-dimensional, water saturated fracture with spatially variable and anisotropic aperture is investigated with a particle tracking model. Both neutrally buoyant and dense colloid suspensions are considered. Although flow and transport in fractured subsurface formations have been studied extensively by numerous investigators, the transport of dense, polydisperse colloid suspensions in a fracture with spatially variable and anisotropic aperture has not been previously explored. Simulated snapshots and breakthrough curves of ensemble averages of several realizations of a log-normally distributed aperture field show that polydisperse colloids exhibit greater spreading than monodisperse colloids, and dense colloids show greater retardation than neutrally buoyant colloids. Moreover, it is demonstrated that aperture anisotropy oriented along the flow direction substantially increases colloid spreading; whereas, aperture anisotropy oriented transverse to the flow direction retards colloid movement.

Key words: colloid transport, fracture, variable aperture, anisotropic aperture field, monodisperse colloids, polydisperse colloids, neutrally buoyant colloids, dense colloids, particle tracking.

Nomenclature

b	local aperture of a fracture (L).
$C_{\ln b}$	covariance function of log-transformed aperture (–).
d_{p}	diameter of a colloid particle (L).
$\mathcal{D}$	molecular diffusion coefficient ($\mathrm{L}^2\mathrm{t}^{-1}$).
g	acceleration due to gravity (Lt^{-2}).
h	piezometric head in the fracture (L).
k	Boltzmann's constant ($\mathrm{ML}^2\mathrm{t}^{-2}\mathrm{T}^{-1}$).
K_{f}	hydraulic conductivity of the fracture (Lt^{-1}).
ℓ_x	fracture length in x-direction (L).
ℓ_y	fracture length in y-direction (L).
m	time step number (–).
M	cumulative colloid mass passing through a cross section of a fracture (M).
M_0	initial mass of suspended colloids (M).
n_x	number of elements along the x-direction of the fracture (–).
n_y	number of elements along the y-direction of the fracture (–).

N	cumulative number of colloids passing through a cross section of a fracture (–).
N_0	total number of colloids introduced into the fracture (–).
$N(d_\mathrm{p})$	number of colloids introduced into the fracture with a given diameter d_p (–).
$P(z)$	probability of a colloid having a starting inlet vertical location $< z$ (–).
r_x	separation distance of fracture aperture measurements in the x-direction (L).
r_y	separation distance of fracture aperture measurements in the y-direction (L).
t	time (t).
T	absolute temperature of the interstitial fluid (T).
U_x	parabolic flow velocity in the x-direction (Lt^{-1}).
$\bar{U}_x$	average flow velocity in the x-direction (Lt^{-1}).
U_y	parabolic flow velocity in the y-direction (Lt^{-1}).
$\bar{U}_y$	average flow velocity in the y-direction (Lt^{-1}).
x	coordinate along the fracture length (L).
y	coordinate along the fracture width (L).
z	coordinate perpendicular to the fracture plane (L).
$Z(0, 1)$	randomly generated number from a normal distribution with zero mean and unit variance (–).

Greek Symbols

γ	fluid specific weight ($\mathrm{ML}^{-2}\mathrm{t}^{-2}$).
Δt	time step (t).
Δz	specified z-direction spatial increment (L).
η	dynamic viscosity of the interstitial fluid ($\mathrm{ML}^{-1}\mathrm{t}^{-1}$).
λ_x	correlation length of the log-transformed aperture fluctuations in the x-direction (L).
λ_y	correlation length of the log-transformed aperture fluctuations in the y-direction (L).
μ_b	mean aperture (L).
μ_{d_p}	mean colloid diameter (L).
$\mu_{\ln d_\mathrm{p}}$	mean log-transformed colloid diameter (–).
ρ_f	interstitial fluid density (ML^{-3}).
ρ_p	colloid particle density (ML^{-3}).
$\sigma^2_{d_\mathrm{p}}$	variance of colloid diameter distribution (L^2).
$\sigma^2_{\ln b}$	variance of log-transformed aperture distribution (–).
$\sigma^2_{\ln d_\mathrm{p}}$	variance of log-transformed colloid diameter distribution (–).
Ω_1, Ω_2	constants (–).

1. Introduction

Colloids derive their name from the Greek word '$\kappa\acute{o}\lambda\lambda\alpha$', meaning 'glue' (Russel *et al.*, 1989) and they are present in the subsurface in the form of very fine particles such as clay minerals, metal oxides, viruses, bacteria, and humic macromolecules (Stumm and Morgan, 1981; Higgo *et al.*, 1993) that generally range in size from 1 nm to 10 μm (Chrysikopoulos and Sim, 1996). In fractured subsurface formations, colloids are produced by microerosion of rock minerals as a result of formation crushing due to tectonic activity (Drever, 1985), chemical dissolution of rock minerals caused by water infiltration, and changes in groundwater geochemical conditions (McCarthy and Degueldre, 1993). Groundwater contaminants often exhibit higher affinity for attachment onto colloids than onto formation solid surfaces (McDowell-Boyer *et al.*, 1986; Toran and Palumbo, 1992). Consequently,

colloids often serve as carriers for contaminants and may significantly influence the net rate of contaminant migration in subsurface formations (Mills *et al.*, 1991; Abdel-Salam and Chrysikopoulos, 1995a; Ouyang *et al.*, 1996; Baik and Hahn, 1997; Tatalovich *et al.*, 2000).

The literature on flow and transport in fractured systems is extensive. Several studies are associated with the relatively simple parallel plate model that represents a fracture as a pair of parallel plates separated by a constant aperture (e.g. Grisak and Pickens, 1981; Neretnieks, 1983; Novakowski *et al.*, 1985; Abdel-Salam and Chrysikopoulos, 1994). Also, numerous are the investigations that explore the relatively complex case of fractures with spatially variable aperture (e.g. Tsang and Tsang, 1987; Moreno *et al.*, 1988; Thompson and Brown, 1991; Johns *et al.*, 1993; Reimus, 1995; Chrysikopoulos and Abdel-Salam, 1997; Keller, 1998; James and Chrysikopoulos, 2000; Knapp *et al.*, 2000). The majority of the mathematical models for colloid transport or contaminant/colloid cotransport in fractured systems assume that colloids are of uniform size (monodisperse colloid suspensions) (e.g. van der Lee *et al.*, 1992; Smith and Degueldre, 1993; Abdel-Salam and Chrysikopoulos, 1995b; Liu *et al.*, 2000; Oswald and Ibaraki, 2001). Because colloids present in groundwaters frequently follow a log-normal distribution in diameter (Ledin *et al.*, 1994), recent studies for colloid transport in fractures based on particle tracking simulations examine the realistic case of variably sized colloid (polydisperse colloid suspensions) transport in water saturated fractures, accounting for both matrix diffusion and colloid deposition (James and Chrysikopoulos, 1999, 2000).

This work extends our previous research efforts and focuses on the transport of monodisperse and polydisperse colloids in a fracture with spatially variable aperture. Colloid suspensions of neutral buoyancy as well as heavier than water (dense) colloids are employed in the model simulations. The effect of fracture aperture anisotropy on colloid transport is investigated. Statistical anisotropy in the fracture aperture distribution is described by a log-normally distributed random field. To our knowledge, the transport of dense, polydisperse colloid suspensions in a fracture with spatially variable and anisotropic aperture has not yet been explored.

2. Mathematical Development

Consider a horizontal, two-dimensional, water saturated fracture plane with length $\ell_x = 8\,\text{m}$ (x-direction), width $\ell_y = 4\,\text{m}$ (y-direction), and spatially variable aperture as shown in Figure 1. The fracture aperture is a stationary log-normally distributed stochastic variable that can be described by an anisotropic exponential covariance function. Water movement is from left to right. No-flow boundary conditions are imposed along the two sides of the fracture ($y = 0$ and $4\,\text{m}$). Flow in the rock matrix is neglected because the saturated hydraulic conductivity in the rock matrix is several orders of magnitude smaller than the saturated hydraulic conductivity within the fracture (Abdel-Salam and Chrysikopoulos, 1996). Colloids

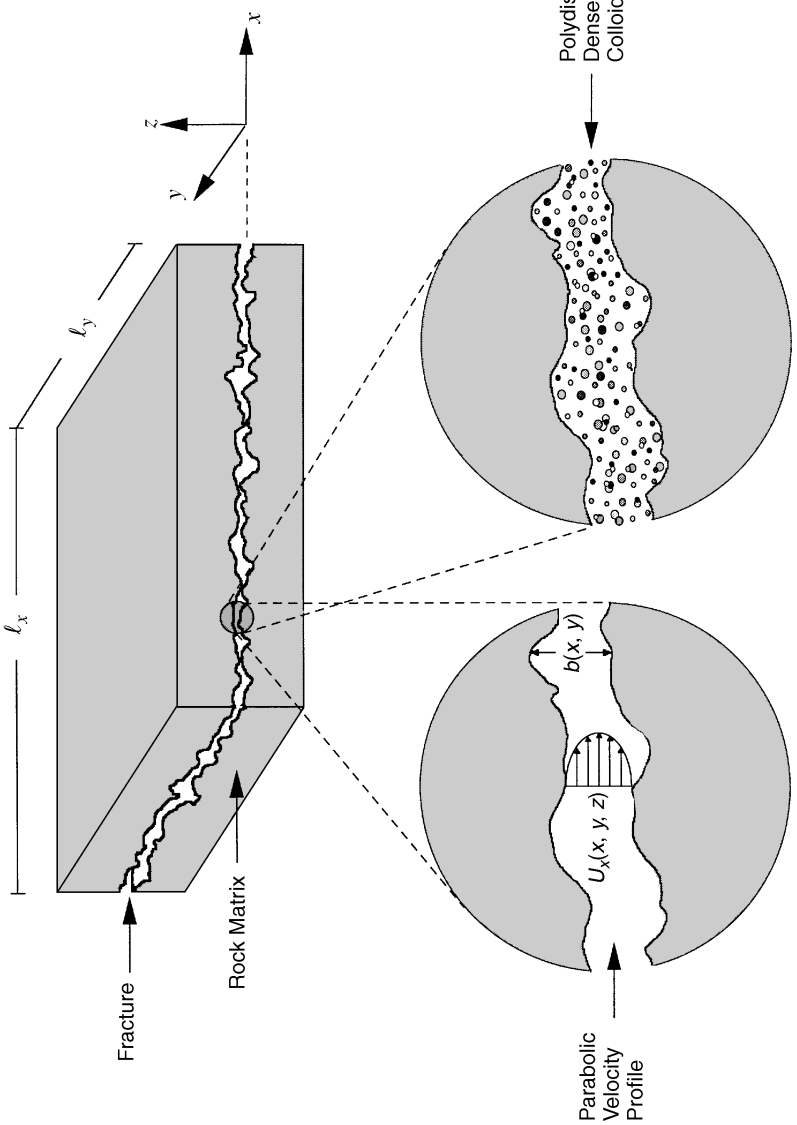

Figure 1. Schematic illustration of a two-dimensional fracture considered in this study showing the spatially variable aperture $b(x, y)$, the fully developed parabolic velocity profile $U(x, y, z)$, and a migrating plume of polydisperse dense colloids. Note that the center of the aperture is located at $z = 0$.

are introduced in proportion to the local flow rate at the upstream inlet and it is assumed that they neither deposit onto the fracture surfaces nor penetrate the solid matrix. Although size exclusion, filtration, and diffusion into the solid matrix can affect colloid transport in a fracture, these factors have been previously examined (Chrysikopoulos and Abdel-Salam, 1997; James and Chrysikopoulos, 1999, 2000) and they are disregarded in this study so that aperture anisotropy in conjunction with gravitational effects on colloids can be explicitly examined. It should be noted that only a horizontal fracture is examined in the present study; however, the case of colloid transport in vertical or inclined fractures will be the focus of a subsequent investigation.

2.1. STOCHASTIC GENERATION OF A FRACTURE PLANE

The two-dimensional fracture plane considered in this study ($\ell_x \times \ell_y = 8 \times 4\,\mathrm{m}^2$) is partitioned into $n_x \times n_y = 80 \times 40$ discrete square elements by superimposing a grid of 3321 (81×41) nodes over the two-dimensional fracture, where n_x and n_y are the number of elements along the x- and y-directions of the fracture, respectively. Each $10 \times 10\,\mathrm{cm}^2$ element is assigned a distinct aperture generated stochastically by the computer program SPRT2D (Gutjahr, 1989). The aperture fluctuations in the fracture plane are log-normally distributed (Johns *et al.*, 1993; Keller, 1998) and the log-transformed aperture varies spatially according to the anisotropic exponential covariance function

$$C_{\ln b}(\mathbf{r}) = \sigma^2_{\ln b} \exp\left[- \left(\frac{r_x^2}{\lambda_x^2} + \frac{r_y^2}{\lambda_y^2} \right)^{1/2} \right], \tag{1}$$

where $\sigma^2_{\ln b}$ is the variance of the log-transformed aperture distribution, $\ln b$; $\mathbf{r} = (r_x, r_y)^{\mathrm{T}}$ is a two-dimensional vector whose magnitude is the separation distance of two aperture measurements; and λ_x and λ_y are the correlation length scales of $\ln b$ in the x- and y-directions, respectively. For distances in the fracture plane smaller than the correlation length, aperture values are likely to be similar, but at distances larger than the correlation length aperture values are uncorrelated. The stochastic realizations of $b(x, y)$ are locally independent of direction; however, anisotropy is introduced globally by the overall spatial variability of the fracture aperture field (Vogler and Chrysikopoulos, 2001). Unique realizations of the aperture field are obtained by changing the seed number supplied to the random field generator.

2.2. FLOW MODEL

The governing two-dimensional partial differential equation describing steady-state fluid flow in a fracture with spatially variable aperture is (Chrysikopoulos and Abdel-Salam, 1997)

$$\frac{\partial}{\partial x}\left[b^3(x, y) \frac{\partial h(x, y)}{\partial x} \right] + \frac{\partial}{\partial y}\left[b^3(x, y) \frac{\partial h(x, y)}{\partial y} \right] = 0, \tag{2}$$

where x is the coordinate along the fracture length, y is the coordinate along the fracture width, and $h(x, y)$ is the local piezometric head in the fracture. The preceding equation is a stochastic partial differential equation, because one of its parameters, namely the local aperture $b(x, y)$, is a stochastic variable.

The appropriate boundary conditions for the fracture are:

$$\frac{\partial h(x, 0)}{\partial y} = 0, \tag{3}$$

$$\frac{\partial h(x, \ell_y)}{\partial y} = 0, \tag{4}$$

$$h(0, y) = h_0, \tag{5}$$

$$h(\ell_x, y) = 0, \tag{6}$$

where h_0 is the constant inlet head potential. Conditions (3) and (4) represent the no-flow top and bottom boundaries, respectively; whereas conditions (5) and (6) represent the constant head left (upstream) and right (downstream) boundaries, respectively. For physical orientation of the fracture, see Figure 1. The direction of the flow is from left to right.

Assuming that the fluid enters the fracture with a fully developed Poiseuille velocity distribution (parabolic velocity profile), no slip boundary conditions exist at the fracture walls, and a fully developed velocity profile forms within each unit element of the fracture plane, the interstitial fluid velocities, U_x and U_y, in the directions along the fracture length and fracture width, respectively, are expressed as (Fox and McDonald, 1998, p. 337; James and Chrysikopoulos, 2000)

$$U_x(x, y, z) = \bar{U}_x(x, y)\frac{3}{2}\left\{1 - 4\left[\frac{z}{b(x, y)}\right]^2\right\}, \tag{7}$$

$$U_y(x, y, z) = \bar{U}_y(x, y)\frac{3}{2}\left\{1 - 4\left[\frac{z}{b(x, y)}\right]^2\right\}, \tag{8}$$

where z is the coordinate perpendicular to the fracture plane, and $\bar{U}_x$ and $\bar{U}_y$ are the average velocity components in the x- and y-directions given by (Chrysikopoulos and Abdel-Salam, 1997)

$$\bar{U}_x(x, y) = -K_f(x, y)\frac{\partial h(x, y)}{\partial x} = -\frac{\gamma b^2(x, y)}{12\eta}\frac{\partial h(x, y)}{\partial x}, \tag{9}$$

$$\bar{U}_y(x, y) = -K_f(x, y)\frac{\partial h(x, y)}{\partial y} = -\frac{\gamma b^2(x, y)}{12\eta}\frac{\partial h(x, y)}{\partial y}, \tag{10}$$

respectively, where γ is the fluid specific weight, η is the fluid dynamic viscosity, and K_f is the hydraulic conductivity of the fracture. For an ideal fracture represented by two parallel plates, the hydraulic conductivity is (Domenico and Schwartz, 1998, p. 51)

$$K_f = \frac{\gamma b^2}{12\eta}. \tag{11}$$

Note that U_x and U_y are functions of the z-coordinate; whereas $\bar{U}_x$ and $\bar{U}_y$ are independent of the z-coordinate.

For each realization of the aperture field, a distribution of the piezometric head within the fracture is obtained by solving the governing fluid flow Equation (2) subject to conditions (3)–(6). A five-point central finite difference numerical approximation is used for each node on the grid of the fracture plane leading to a set of linear equations with as many unknowns as the number of unspecified nodes on the fracture grid (Hoffman, 1992). The resulting set of linear equations is solved using a banded LU decomposition matrix solver algorithm (Press *et al.*, 1992). Because lubrication theory is used to calculate flow between fracture elements, a step discontinuity may not be explicitly modeled. Therefore, the equivalent aperture between adjacent elements, in x- or y-direction, is approximated by the harmonic mean (Reimus, 1995). The directional components of the average velocity within each element are generated by second-order accurate finite difference approximations of (9) and (10); and the corresponding local, directional interstitial velocities are evaluated from (7) and (8).

2.3. MODELING OF COLLOID TRANSPORT BY PARTICLE TRACKING

Numerous published studies focus on modeling colloid transport in fractures and use various analytical and numerical solution techniques for the governing partial differential equations. Analytical solutions are applied to simple physicochemical conditions and fracture geometries (de Marsily, 1986, p. 268; Abdel-Salam and Chrysikopoulos, 1994), more complex situations require finite element or finite difference approximations that suffer from numerical dispersion (van der Lee *et al.*, 1992; Smith and Degueldre, 1993; Abdel-Salam and Chrysikopoulos, 1995a, b; Ibaraki and Sudicky, 1995; Chrysikopoulos and Abdel-Salam, 1997), and other investigations employ particle tracking techniques that require significant computational power (Reimus, 1995; Grindrod and Lee, 1997; James and Chrysikopoulos, 1999, 2000). In this study, colloid transport is simulated with particle tracking. Particle tracking is the only method that can account for both variably sized (polydisperse) colloids and irregular boundaries (spatially variable aperture), because a unique set of parameters is allocated to each particle to store its permanent and continuously changing characteristics (e.g. location, size, sorption status, and gravitational properties). Furthermore, particle tracking procedures provide stochastic

solutions to linear partial differential equations that do not suffer from numerical dispersion (Thompson and Gelhar, 1990).

Traditional particle tracking equations for colloid transport in water saturated fractures simulate spatial particle advancements over a constant time step. They consist of two terms: a deterministic term representing advection processes, and a stochastic term simulating random molecular diffusion. However, traditional particle tracking equations with a constant time step may be inappropriate for polydisperse colloids, because during the pre-determined time step, a small particle will experience a significantly greater diffusional effect than a large particle. By specifying a priori a spatial step for transport across streamlines and determining the random time required by each particle to travel this distance, the movement of small and large colloids is modeled with equal accuracy. In this work, the constant spatial step particle tracking equations derived by James and Chrysikopoulos (2001) are employed.

2.3.1. *Transport of Neutrally Buoyant Colloids*

For neutrally buoyant polydisperse colloid plumes each particle is transported through the water saturated fracture according to the following equations:

$$x^m = x^{m-1} + U_x(x^{m-1}, y^{m-1}, z^{m-1})\Delta t + Z(0,1)\sqrt{2\mathcal{D}\Delta t}, \tag{12}$$

$$y^m = y^{m-1} + U_y(x^{m-1}, y^{m-1}, z^{m-1})\Delta t + Z(0,1)\sqrt{2\mathcal{D}\Delta t}, \tag{13}$$

$$z^m = z^{m-1} \pm \Delta z, \tag{14}$$

where $Z(0,1)$ is a random selection from the standard normal distribution with zero mean and unit variance, m is the spatial step level, and $\mathcal{D}$ is the molecular diffusion coefficient specified for a spherical particle by the Stokes–Einstein diffusion equation (Russel *et al.*, 1989, p. 69)

$$\mathcal{D} = \frac{kT}{3\pi\eta d_p}, \tag{15}$$

where d_p is the particle diameter, k is Boltzmann's constant, and T is the temperature of the interstitial fluid. The direction of the displacement $\pm\Delta z$ in (14) is determined from the sign of another standard normally distributed random number, $Z(0,1)$. The time step Δt employed in (12) and (13) is calculated by (James and Chrysikopoulos, 2001)

$$\Delta t = \exp\left\{\ln\left[\frac{(\Delta z)^2}{\mathcal{D}}\right] - \Omega_1 + \Omega_2 \cdot Z(0,1)\right\}, \tag{16a}$$

$$\Omega_1 = 0.979 \pm 0.012, \tag{16b}$$

$$\Omega_2 = 0.787 \pm 0.002. \tag{16c}$$

The preceding set of equations represents a random selection of Δt from the log-normal distribution of the travel times for a particle with molecular diffusion coefficient $\mathcal{D}$ traveling a distance Δz. Following the selection of an appropriate value for Δz and substitution of (15) into (16a), a random time step Δt is calculated and used in both (12) and (13). It should be noted that for traditional particle tracking with constant time step, (14) should be replaced by

$$z^m = z^{m-1} + Z(0, 1)\sqrt{2\mathcal{D}\Delta t}. \tag{17}$$

2.3.2. *Transport of Dense Colloids*

For polydisperse colloid plumes subject to gravitational forces the effects of gravitational settling on each colloid must be incorporated into the particle tracking equations. Assuming that a colloid is reasonably represented by a small sphere, for a density difference between the colloid and the suspending fluid, the balance among gravity, buoyancy, and viscous forces leads to the following expression for the terminal settling velocity (Russel *et al.*, 1989, p. 395)

$$U_s = -\frac{(\rho_p - \rho_f) g d_p^2}{18\eta}, \tag{18}$$

where ρ_f and ρ_p are the densities of the suspending fluid and the colloid particle, respectively, and g is the acceleration due to gravity in the negative z-direction.

The transport of colloids in the x- and y-directions is not affected by gravitational settling. Consequently, the appropriate particle tracking equations for dense colloids are (12), (13) and

$$z^m = z^{m-1} \pm \Delta z + U_s \Delta t, \tag{19}$$

where the direction of the displacement $\pm\Delta z$ is determined again from the sign of a standard normally distributed random number, $Z(0, 1)$. Selecting an appropriate value for Δz and substituting (15) into (16a), a random time step Δt is determined to be employed in (12), (13), and (19).

2.3.3. *Colloid Transport Modeling Procedures*

The procedure used for the distribution of colloid particles at the upstream boundary of the fracture ($x = 0$) is essentially identical to that employed by Reimus (1995). The probability of a particle entering a given element at the upstream boundary is proportional to the volumetric flow rate into that element ($U_x b \ell_y / n_y$, here $\ell_y / n_y = 10\,\text{cm}$), and consequently proportional to the aperture, b, of that element. A discrete cumulative probability density function is specified by sequentially adding the probabilities of a particle entering each of the n_y elements at the upstream boundary of the fracture. The probability of a particle entering a given element is equal to the volumetric flow rate of that element divided by the sum of

the n_y individual volumetric flow rates passing through the upstream boundary of the fracture. A uniform random number between zero and 1 is generated for each particle. The random number's placement in the discrete cumulative distribution designates a particle's appropriate entrance element at the upstream boundary. In addition to assigning an entrance element, a starting z-location (perpendicular to the fracture walls) is also assigned for each particle because different vertical locations correspond to different local interstitial fluid velocities (parabolic velocity profile) within each inlet element of the fracture. The probability of a colloid having a starting position less than z is given by (Reimus, 1995)

$$P(z) = \frac{\int_{-b/2}^{z} U_x(0, y, z)\,\mathrm{d}z}{\int_{-b/2}^{b/2} U_x(0, y, z)\,\mathrm{d}z} = -\frac{2z^3}{b^3(0, y)} + \frac{3z}{2b(0, y)} + \frac{1}{2}, \tag{20}$$

where the last formulation in the preceding equation is the consequence of employing (7) followed by evaluation of the integrals. A uniform random number between zero and 1 is substituted for $P(z)$ in (20) and the roots of the resulting polynomial in z are evaluated by Newton's method (Press *et al.*, 1992, p. 355). Roots found outside the range of $-b(0, y)/2$ and $b(0, y)/2$ are ignored and particles overlapping with the fracture wall have their positions reevaluated with a new random number. Note that particle–particle interactions are not considered in this study.

Particle movement between elements of different aperture follows the relationship (Happel and Brenner, 1965):

$$\frac{z_{\text{old}}}{b_{\text{old}}} = \frac{z_{\text{new}}}{b_{\text{new}}}, \tag{21}$$

that is applicable for creeping flow conditions in slowly converging or diverging channels. Thus the ratio of the new z-location to the old z-location is equivalent to the ratio of the aperture at the new location to the aperture at the old location. It should be noted that the preceding equations implicitly assumes that a colloid particle moving between elements with the local advection velocity follows directly a streamline. Particles are allowed to cross both perpendicularly as well as diagonally between cells; however, if a particle crosses diagonally only its initial and final element apertures are used in (21).

For the present study the fracture walls are considered impermeable to colloids. Consequently, it is assumed that when particles encounter fracture walls they are reflected back as in a mirror image without loss of energy. That is, the final x- and y-coordinate positions remain unchanged, whereas the final z-coordinate is set a distance away from the wall equal to the distance that the particle would have obtained if it had penetrated the rock matrix plus the particle diameter. For example, if a particle of $d_{\text{p}} = 1 \times 10^{-6}$ m is initially estimated to move to a z-location of 5.03×10^{-5} m (5.0×10^{-5} m being the location of the fracture wall), its reflected z-location would be 4.87×10^{-5} m. Also, it should be noted that the center of a colloid particle may not reach the location $z = 0$ due to its finite size. Therefore,

near the fracture wall a colloid may move by diffusion as well as advection because its velocity component, U_x, although very small, is never equal to zero.

3. Model Parameters

One monodisperse and two polydisperse colloid plumes are employed for the model simulations. Each plume consists of a total number of $N_0 = 10,000$ colloids. Assuming that the colloid particles are spherical, the mass of each colloid suspension is

$$M_0 = \frac{\rho_p \pi}{6} \sum_{i=1}^{N_0} d_{p_i}^3. \tag{22}$$

A relatively large number of particles is used for the model simulations presented in this study to reduce random noise. The larger the number of particles, the smaller the contribution of each particle to the overall transport behavior of a colloid plume, and thus the smoother the results. All colloid suspensions have the same mean colloid diameter, $\mu_{d_p} = 1\,\mu\text{m}$. However, the two polydisperse colloid suspensions with standard deviation of colloid diameters $\sigma_{d_p} = 0.9$ and $1.8\,\mu\text{m}$, respectively, are assumed to follow a log-normal size distribution (Ang and Tang, 1975)

$$N(d_p) = \frac{N_0}{(2\pi)^{1/2}\sigma_{\ln d_p} d_p} \exp\left[-\frac{1}{2}\left(\frac{\ln d_p - \mu_{\ln d_p}}{\sigma_{\ln d_p}}\right)^2\right], \tag{23}$$

where $N(d_p)$ is the number of colloids with a given diameter d_p, $\mu_{\ln d_p}$ is the mean log-transformed colloid diameter, and $\sigma^2_{\ln d_p}$ is the variance of the log-transformed colloid diameter distribution. Note that the mean colloid diameter is represented by

$$\mu_{d_p} = \exp\left[\mu_{\ln d_p} + 0.5\sigma^2_{\ln d_p}\right], \tag{24}$$

and the variance of the colloid diameter distribution by

$$\sigma^2_{d_p} = \mu^2_{d_p}(e^{\sigma^2_{\ln d_p}} - 1). \tag{25}$$

Unique realizations of the aperture field for the fracture considered in this study are determined with a mean aperture $\mu_b = 5 \times 10^{-5}\,\text{m}$, a variance of the log-transformed aperture distribution $\sigma^2_{\ln b} = 0.2$, and three different combinations of the directional correlation length scales of the log-transformed aperture field (λ_x, λ_y). Table I presents the various correlation length scales and their ratios, λ_x/λ_y. It should be noted that the correlation lengths of $\ln b$ employed in this work were arbitrarily selected. For each realization of the aperture field, the corresponding directional components of the interstitial velocity (U_x, U_y) at each unit element are determined for a hydraulic gradient of $\partial h/\partial x = 0.031$, imposed by an upstream boundary condition $h(0, y) = h_0 = 0.25\,\text{m}$ and a downstream boundary condition

Table I. Correlation lengths of $\ln b$ for model simulations

λ_x (cm)	λ_y (cm)	Ratio
100	500	0.2
100	100	1.0
500	100	5.0

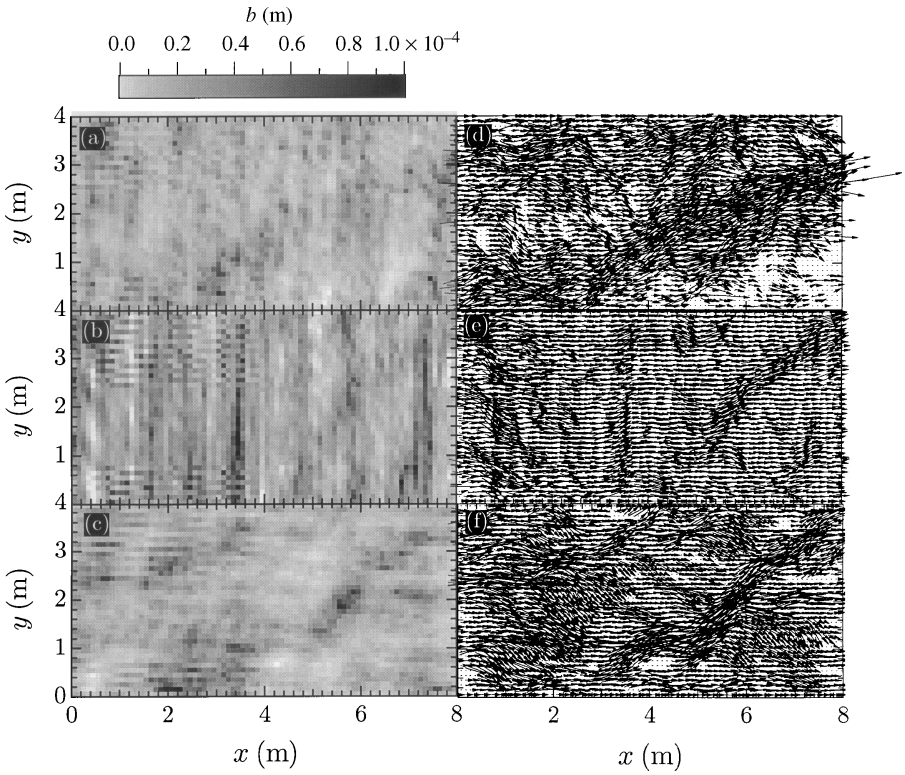

Figure 2. Illustration of statistically anisotropic aperture field realizations for: (a) $\lambda_x = 100\,\text{cm}$, $\lambda_y = 100\,\text{cm}$; (b) $\lambda_x = 100\,\text{cm}$, $\lambda_y = 500\,\text{cm}$ and (c) $\lambda_x = 500\,\text{cm}$, $\lambda_y = 100\,\text{cm}$. The velocity vector field (d) corresponds to the aperture field (a); the velocity vector field (e) corresponds to the aperture field (b); and velocity vector field (f) corresponds to the aperture field (c). Arrow lengths are proportional to velocity magnitudes (here $\mu_b = 5 \times 10^{-5}\,\text{m}$, $\sigma^2_{\ln b} = 0.2$, $\partial h/\partial x = 0.031$; flow direction from left to right).

$h(\ell_x, y) = 0\,\text{m}$ for $\ell_x = 8\,\text{m}$. Figure 2 shows three realizations of the aperture field and the corresponding velocity vector fields.

For the particle tracking method employed here a constant spatial step in the z-direction, Δz, equal to one-fifth of the local aperture ($\Delta z = b(x, y)/5$) is used for neutrally buoyant colloids and one-tenth of the local aperture ($\Delta z = b(x, y)/10$) for dense colloids. These spatial steps were carefully chosen to assure reasonable

accuracy from the particle tracking procedures by not allowing a time step that would have a neutrally buoyant particle travel across multiple elements in either the x- or y-direction, or a dense particle to travel across the fracture due to gravitational forces.

4. Model Simulations

Model simulations for the transport of neutrally buoyant, as well as dense, polydisperse colloids in a fracture with spatially variable, anisotropic aperture are performed for a variety of situations. Unless otherwise specified, the results presented here represent the ensemble average from 100 realizations of the fracture aperture field. The number of realizations is chosen such that additional realizations do not change the calculated ensemble average by more than 1%. Colloid number breakthrough curves represent the cumulative number of colloids passing through the downstream boundary of the fracture at $x = 8\,\mathrm{m}$, and they are normalized by the total number of colloids introduced into the fracture (N/N_0). Colloid mass breakthrough curves represent the cumulative mass of colloids passing through the downstream boundary of the fracture and they are normalized by the initial mass of suspended colloids introduced into the fracture (M/M_0), and in view of (22) can be expresses as

$$\frac{M}{M_0} = \frac{\sum_{i=1}^{N} d_{\mathrm{p}i}^3}{\sum_{i=1}^{N_0} d_{\mathrm{p}i}^3}. \tag{26}$$

4.1. MONODISPERSE COLLOIDS

Figure 3 qualitatively illustrates the effect of colloid density as well as fracture aperture anisotropy on the transport of monodisperse colloids in water saturated fractures with spatially variable aperture. Snapshots of 10,000 monodisperse particles are presented at 12 h (solid circles) and 36 h (open squares) of transport times for six different cases. The first case (Figure 3(a)) represents transport of monodisperse, neutrally buoyant colloids ($\rho_{\mathrm{p}} = 1000\,\mathrm{kg/m^3}$) in a fracture with spatially variable and isotropic aperture distribution, as shown in Figure 2(a). The second case (Figure 3(b)) represents transport of monodisperse, neutrally buoyant colloids in a fracture with spatially variable and anisotropic aperture distribution, as shown in Figure 2(b). The third case (Figure 3(c)) represents transport of monodisperse, neutrally buoyant colloids in a fracture with spatially variable and anisotropic aperture distribution, as shown in Figure 2(c). The fourth, fifth and sixth cases (Figure 3(d)–(f)) represent transport of monodisperse, dense colloids ($\rho_{\mathrm{p}} = 2000\,\mathrm{kg/m^3}$) for the fracture topographies examined in Figure 3(a), (b) and (c), respectively. Comparison of the six cases suggests that dense, monodisperse colloids show significant retardation and less spreading because they are likely

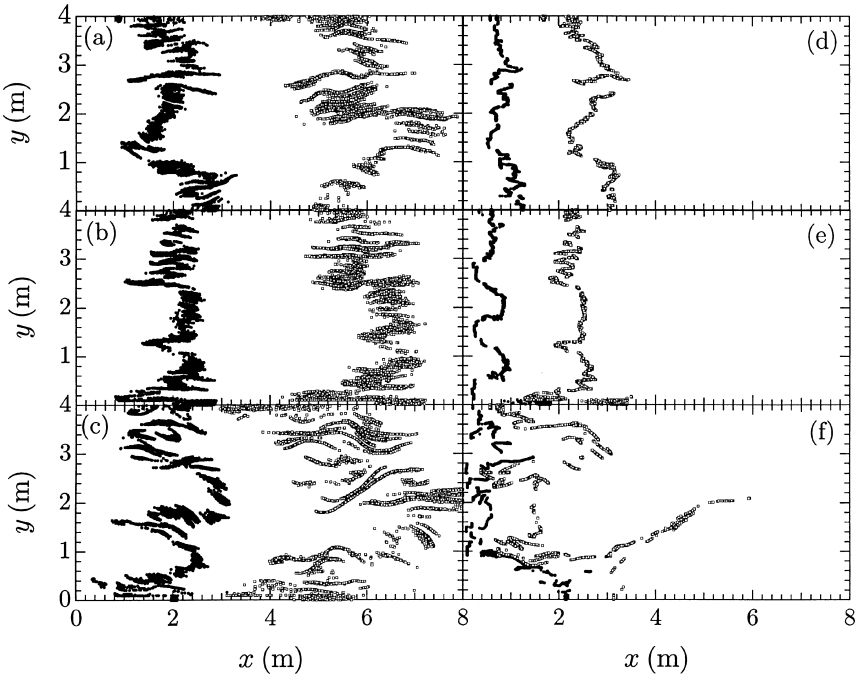

Figure 3. Snapshots of monodisperse colloid positions at 12 h (solid circles) and 36 h (open squares) of transport times for: (a) neutrally buoyant colloids and isotropic aperture distribution with $\lambda_x/\lambda_y = 1.0$; (b) neutrally buoyant colloids and anisotropic aperture distribution with $\lambda_x/\lambda_y = 0.2$; (c) neutrally buoyant colloids and anisotropic aperture distribution with $\lambda_x/\lambda_y = 5.0$; (d) dense colloids and isotropic aperture distribution with $\lambda_x/\lambda_y = 1.0$; (e) dense colloids and anisotropic aperture distribution with $\lambda_x/\lambda_y = 0.2$; and (f) dense colloids and anisotropic aperture distribution with $\lambda_x/\lambda_y = 5.0$ (here $d_\mathrm{p} = 1\,\mu\mathrm{m}$, $\sigma_{d_\mathrm{p}} = 0.0\,\mu\mathrm{m}$, $\mu_b = 5 \times 10^{-5}$ m, $\sigma^2_{\ln b} = 0.2$).

to travel near the bottom of the fracture thereby experiencing a narrow range of smaller flow velocities. Furthermore, it is shown that anisotropy in the spatially variable aperture field oriented along the flow direction increases the spreading of the monodisperse colloid plumes; whereas aperture anisotropy oriented transverse to the flow direction retards colloid movement. This observation agrees with the transport results for monodisperse, neutrally buoyant colloids of Thompson and Brown (1991).

4.2. POLYDISPERSE COLLOIDS

Figure 4 qualitatively illustrates the effect of colloid density as well as fracture aperture anisotropy on the transport of polydisperse colloids in water saturated fractures with spatially variable aperture. Snapshots of 10,000 polydisperse particles with $\sigma_{d_\mathrm{p}} = 1.8\,\mu\mathrm{m}$ are presented at 12 h (solid circles) and 36 h (open squares) of transport simulated times for six different cases. The first case (Figure 4(a)) represents transport of polydisperse, neutrally buoyant colloids ($\rho_\mathrm{p} = 1000\,\mathrm{kg/m^3}$)

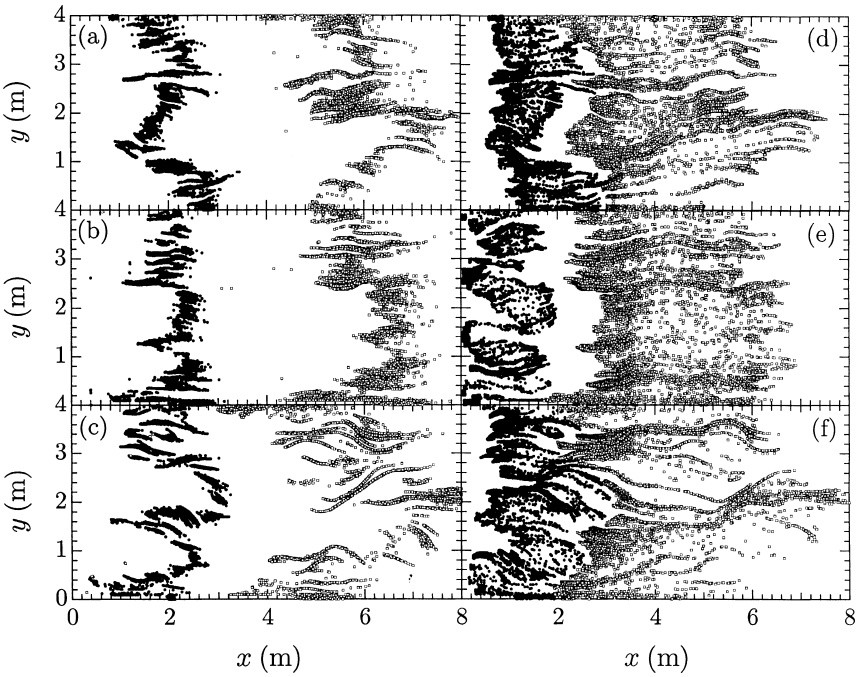

Figure 4. Snapshots of polydisperse colloid positions at 12 h (solid circles) and 36 h (open squares) of transport times for: (a) neutrally buoyant colloids and isotropic aperture distribution with $\lambda_x/\lambda_y = 1.0$; (b) neutrally buoyant colloids and anisotropic aperture distribution with $\lambda_x/\lambda_y = 0.2$; (c) neutrally buoyant colloids and anisotropic aperture distribution with $\lambda_x/\lambda_y = 5.0$; (d) dense colloids and isotropic aperture distribution with $\lambda_x/\lambda_y = 1.0$; (e) dense colloids and anisotropic aperture distribution with $\lambda_x/\lambda_y = 0.2$; and (f) dense colloids and anisotropic aperture distribution with $\lambda_x/\lambda_y = 5.0$ (here $\mu_{d_p} = 1\,\mu\text{m}$, $\sigma_{d_p} = 1.8\,\mu\text{m}$, $\mu_b = 5 \times 10^{-5}$ m, $\sigma^2_{\ln b} = 0.2$).

in a fracture with spatially variable and isotropic aperture distribution, as shown in Figure 2(a). The second case (Figure 4(b)) represents transport of polydisperse, neutrally buoyant colloids in a fracture with spatially variable and anisotropic aperture distribution, as shown in Figure 2(b). The third case (Figure 4(c)) represents transport of polydisperse, neutrally buoyant colloids in a fracture with spatially variable and anisotropic aperture distribution, as shown in Figure 2(c). The fourth, fifth and sixth cases (Figure 4(d)–(f)) represent transport of polydisperse, dense colloids ($\rho_p = 2000\,\text{kg/m}^3$) for the fracture topographies examined in Figure 4(a), (b) and (c), respectively. Comparison of the six cases suggests that the center of mass of the dense, polydisperse colloid suspensions is more retarded than the center of mass of the neutrally buoyant, polydisperse colloids. Furthermore, aperture anisotropy oriented along the flow direction increases the spreading of the polydisperse colloid plumes and aperture anisotropy oriented transverse to the flow direction inhibits colloid movement. Examining Figures 3 and 4 reveals that polydisperse colloids spread to a greater degree than monodisperse colloids, because the

many small colloids of a polydisperse suspension are less affected by gravitational forces and they can sample the whole range of a parabolic velocity distribution of the fracture. Furthermore, the largest colloids of the distribution are most affected by gravitational forces and travel according to the slowest portion of the parabolic velocity profile.

4.3. MASS AND COLLOID NUMBER BREAKTHROUGH CURVES

Cumulative breakthrough curves for various colloid distributions and fracture topographies are presented in Figure 5. Normalized colloid mass breakthrough curves are presented in Figure 5(b) and (e), and normalized colloid number breakthrough curves are presented in Figure 5(a), (c), (d) and (f). The breakthrough curves on the left-hand side (Figure 5(a)–(c)) correspond to neutrally buoyant colloids ($\rho_{\mathrm{p}} = 1000\,\mathrm{kg/m^3}$), whereas the breakthrough curves on the right-hand side (Figure 5(d)–(f)) correspond to dense colloids ($\rho_{\mathrm{p}} = 2000\,\mathrm{kg/m^3}$). In Figure 5(a), the colloid breakthrough curves are nearly identical showing that polydispersity does not affect the number breakthrough of neutrally buoyant particles in isotropic

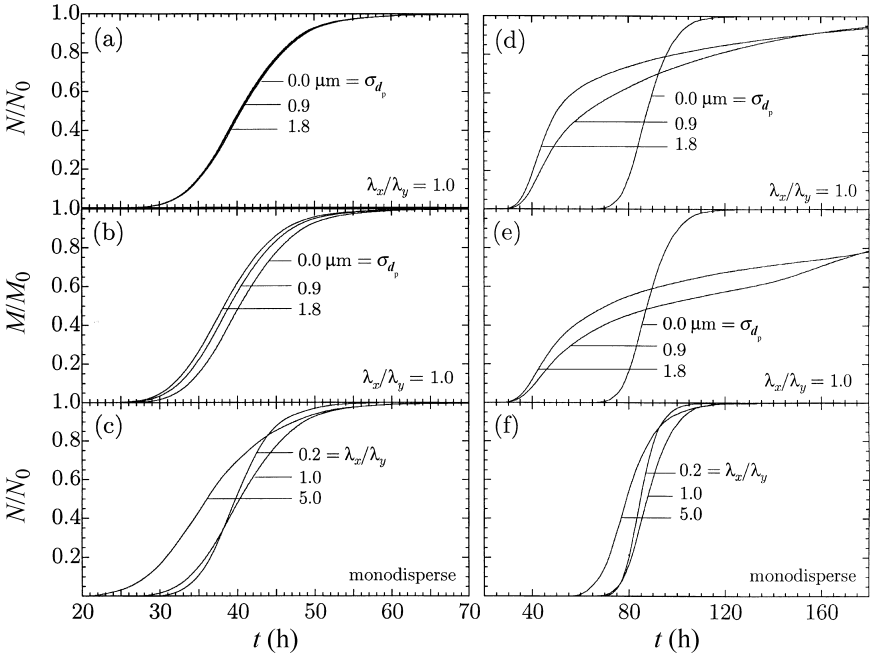

Figure 5. Cumulative normalized colloid number breakthrough curves (a, c, d and f) and cumulative normalized mass breakthrough curves (b and e). Various polydisperse colloid distributions and fractures with isotropic aperture distributions are considered in (a, b, d and e); whereas a monodisperse colloid distribution and fractures with various anisotropic aperture distributions are considered in (c and f). Neutrally buoyant colloids are considered in (a–c) and dense colloids in (d–f). All breakthrough curves are ensemble averages of 100 realizations of the fracture aperture field (here $\mu_{d_{\mathrm{p}}} = 1\,\mu\mathrm{m}$, $\mu_b = 5 \times 10^{-5}\,\mathrm{m}$, $\sigma^2_{\ln b} = 0.2$).

fractures. The normalized mass breakthrough curves of neutrally buoyant colloids in Figure 5(b) indicate that the earliest colloid mass breakthrough corresponds to the colloid plume with the largest $\sigma^2_{d_p}$. It should be noted that large colloids, due to their size, are physically excluded from the slowest moving portion of the velocity profile nearest to the wall and remain in high velocity streamlines near the center of the fracture longer than the small particles due to their lower diffusivity. Figure 5(c) suggests that aperture anisotropy oriented along the flow direction increases the spreading of monodisperse colloid suspensions and aperture anisotropy oriented transverse to the flow direction inhibits colloid transport. Comparison of Figure 5(a) and (b) with Figure 5(d) and (e) indicates that the center of mass for dense, variably sized colloid suspensions moves much slower than the center of mass for neutrally buoyant colloid suspensions. Furthermore, it is shown that dense, polydisperse colloid suspensions disperse considerably more than neutrally buoyant colloid suspensions. Comparison of Figure 5(c) with Figure 5(f) also reveals that the transport of dense, monodisperse colloid suspensions is significantly retarded compared to the neutrally buoyant, monodisperse colloid suspensions. It should be noted that the colloid breakthrough curves presented in Figure 5(c) lead to the same results as the transport simulations illustrated in Figure 3(a)–(c). Also, the colloid breakthrough curves presented in Figure 5(f) lead to the same results as the transport simulations illustrated in Figure 3(d)–(f).

5. Summary

The transport of monodisperse and polydisperse colloid suspensions in water saturated, two-dimensional fractures with different spatially variable, anisotropic aperture topographies was simulated with a particle tracking model. The governing two-dimensional partial differential equation describing steady-state fluid flow in the fracture was solved for various realizations of the spatially variable aperture field by a five-point finite difference numerical approximation; whereas the transport of colloid suspensions was determined by appropriate particle tracking equations with a constant spatial step. Results from model simulations show that polydisperse colloid suspensions exhibit more spreading than monodisperse suspensions, and that the transport of dense colloid suspensions is retarded compared to neutrally buoyant colloid suspensions. Furthermore, it was demonstrated that aperture anisotropy oriented along the flow direction increases the spreading of both monodisperse and polydisperse colloid suspensions; whereas aperture anisotropy oriented transverse to the flow direction inhibits the transport of colloid suspensions.

Acknowledgement

This work was partially sponsored by Sandia National Laboratories operated by Sandia Corporation, a Lockheed Martin Company, for the United States Department of Energy under contract DE-AC04-94AL85000.

References

Abdel-Salam, A. and Chrysikopoulos, C. V.: 1994, Analytical solutions for one-dimensional colloid transport in saturated fractures, *Adv. Water Resour.* **17**, 283–296.

Abdel-Salam, A. and Chrysikopoulos, C. V.: 1995a, Modeling of colloid and colloid-facilitated contaminant transport in a two-dimensional fracture with spatially variable aperture, *Transport in Porous Media* **20**, 197–221.

Abdel-Salam, A. and Chrysikopoulos, C. V.: 1995b, Analysis of a model for contaminant transport in fractured media in the presence of colloids, *J. Hydrol.* **165**, 261–281.

Abdel-Salam, A. and Chrysikopoulos, C. V.: 1996, Unsaturated flow in a quasi-three-dimensional fractured medium with spatially variable aperture, *Water Resour. Res.* **32**(6), 1531–1540.

Ang, A. H.-S. and Tang, W. H.: 1975, *Probability Concepts in Engineering Planning and Design*, Volume 1, *Basic Principles*, Wiley, New York, NY, p. 409.

Baik, M. H. and Hahn, P. S.: 1997, Radionuclide transport facilitated by polydispersed pseudo-colloids in the fractured rock media, *J. Nucl. Sci. Technol.* **34**(1), 41–49.

Chrysikopoulos, C. V. and Abdel-Salam, A.: 1997, Modeling colloid transport and deposition in saturated fractures, *Colloids Surf. A: Physicochem. Eng. Aspects* **121**, 189–202.

Chrysikopoulos, C. V. and Sim, Y.: 1996, One-dimensional virus transport in homogeneous porous media with time dependent distribution coefficient, *J. Hydrol.* **185**, 199–219.

de Marsily, G.: 1986, *Quantitative Hydrogeology: Groundwater Hydrology for Engineers*, Academic Press, San Diego, CA, p. 440.

Domenico, P. A. and Schwartz, F. W.: 1998, *Physical and Chemical Hydrogeology*, 2nd edn., Wiley, New York, NY, p. 506.

Drever, J. I.: 1985, *The Chemistry of Weathering*, NATO ASI Series. Series C, *Mathematical and Physical Sciences*, Vol. 149, Reidel, Dordrecht, Holland, p. 325.

Fox, R. W. and McDonald, A. T.: 1998, *Introduction to Fluid Mechanics*, 5th edn., Wiley, New York, NY, p. 762.

Grindrod, P. and Lee, A. J.: 1997, Colloid migration in symmetrical non-uniform fractures: Particle tracking in three dimensions, *J. Contam. Hydrol.* **27**, 157–175.

Grisak, G. E. and Pickens, J. F.: 1981, An analytical solution for solute transport through fractured media with matrix diffusion, *J. Hydrol.* **52**, 47–57.

Gutjahr, A. L.: 1989, Fast Fourier transform for random field generation, Report 4-R58-2690R, New Mexico Institute of Mining and Technology, Socorro, NM.

Happel, J. and Brenner, H.: 1965, *Low Reynolds Number Hydrodynamics with Applications to Particulate Media*, Prentice-Hall, Englewood Cliffs, NJ, p. 553.

Higgo, J. J. W., Williams, G. M., Harrison, I., Warwick, P., Gardiner, M. P. and Longworth, G.: 1993, Colloid transport in a glacial sand aquifer, laboratory and field studies, *Colloids Surf. A: Physicochem. Eng. Aspects* **73**, 179–200.

Hoffman, J. D.: 1992, *Numerical Methods for Engineers and Scientists*, McGraw-Hill, New York, NY, p. 825.

Ibaraki, M. and Sudicky, E. A.: 1995, Colloid-facilitated contaminant transport in discretely fractured porous media. 1. Numerical formulation and sensitivity analysis, *Water Resour. Res.* **31**(12), 2945–2960.

James, S. C. and Chrysikopoulos, C. V.: 1999, Transport of polydisperse colloid suspensions in a single fracture, *Water Resour. Res.* **35**(3), 707–718.

James, S. C. and Chrysikopoulos, C. V.: 2000, Polydisperse colloid transport through a variable aperture fracture, *Water Resour. Res.* **36**(6), 1457–1466.

James, S. C. and Chrysikopoulos, C. V.: 2001, An efficient particle tracking equation with specified spatial step for the solution of the diffusion equation, *Chem. Eng. Sci.* **56**(23), 6535–6543.

Johns, R. A., Steade, J. S., Costanier, L. M. and Roberts, P. V.: 1993, Nondestructive measurements of fracture aperture in crystalline rock cores using X-ray computed tomography, *J. Geophys. Res.* **98**(B2), 1889–1900.

Keller, A. A.: 1998, High resolution non-destructive measurement and characterization of fracture apertures, *Int. J. Rock Mech. Min. Sci.* **35**(8), 1037–1050.

Knapp, R. B., Chiarappa, M. L. and Durham, W. B.: 2000, An experimental exploration of the transport and capture of abiotic colloids in a single fracture, *Water Res.* **36**(11), 3139–3149.

Ledin, A., Karlsson, S., Duker, A. and Allard, B.: 1994, Measurements in situ of concentration and size distribution of colloidal matter in deep groundwater by photon correlation spectroscopy, *Water Res.* **28**(7), 1539–1545.

Liu, H. H., Bodvarrson, G. S. and Pan, L.: 2000, Determination of particle transfer in random walk particle methods for fractured porous media, *Water Resour. Res.* **36**(3), 707–713.

McCarthy, J. F. and Degueldre, C.: 1993, in: J. Buffle and H. P. van Leeuwen (eds), *Environmental Particles*, Chap. 6, Vol. 2, Lewis, Boca Raton, FL, p. 247.

McDowell-Boyer, L. M., Hunt, J. R. and Sitar, N.: 1986, Particle transport through porous media, *Water Resour. Res.* **22**, 1901–1921.

Mills, W. B., Liu, S. and Fong, F. K.: 1991, Literature review and model (COMET) for colloid/metals transport in porous media, *Ground Water* **29**(2), 199–208.

Moreno, L., Tsang, Y. W., Tsang, C. F., Hale, F. V. and Neretnieks, I.: 1988, Flow and tracer transport in a single fracture: A stochastic model and its relation to some field observations, *Water Resour. Res.* **24**, 2033–2048.

Neretnieks, I.: 1983, A note on fracture flow dispersion mechanisms in the ground, *Water Resour. Res.* **23**, 561–570.

Novakowski, K. S., Evans, G. V., Lever, D. A. and Raven, K.: 1985, A field example of measuring hydrodynamic dispersion in a single fracture, *Water Resour. Res.* **21**, 1165–1174.

Oswald, J. G. and Ibaraki, M.: 2001, Migration of colloids in discretely fractured porous media: Effect of colloidal matrix diffusion, *J. Contam. Hydrol.* **52**, 213–244.

Ouyang, Y., Shinde, D., Mansell, R. S. and Harris, W.: 1996, Colloid-enhanced transport of chemicals in subsurface environments – A review, *Crit. Rev. Environ. Sci. Technol.* **26**(2), 189–204.

Press, W., Teukolsky, S., Vetterling, W. and Flannery, B.: 1992, *Numerical Recipes in FORTRAN – The Art of Scientific Computing*, 2nd edn., Cambridge University Press, Cambridge, UK, p. 963.

Reimus, P. W.: 1995, The use of synthetic colloids in tracer transport experiments in saturated rock fractures, Report LA-13004-T, Los Alamos National Laboratory, Los Alamos, NM.

Russel, W. B., Saville, D. A. and Schowalter, W. R.: 1989, *Colloidal Dispersions*, Cambridge University Press, Cambridge, UK, p. 525.

Smith, P. A. and Degueldre, C.: 1993, Colloid-facilitated transport of radionuclides through fractured media, *J. Contam. Hydrol.* **13**, 143–166.

Stumm, W. and Morgan, J. J.: 1981, *Aquatic Chemistry: An Introduction Emphasizing Chemical Equilibria in Natural Waters*, 2nd edn., Wiley, New York, NY, p. 780.

Tatalovich, M. E., Lee, K. Y. and Chrysikopoulos, C. V.: 2000, Modeling the transport of contaminants originating from the dissolution of DNAPL pools in aquifers in the presence of dissolved humic substances, *Transport in Porous Media* **38**(1/2), 93–115.

Thompson, M. E. and Brown, S. R.: 1991, The effect of anisotropic surface roughness on flow and transport in fractures, *J. Geophys. Res.* **96**(B13), 21923–21932.

Thompson, A. F. B. and Gelhar, L. W.: 1990, Numerical simulation of solute transport in three-dimensional, randomly heterogeneous porous media, *Water Resour. Res.* **26**(10), 2541–2562.

Toran, L. and Palumbo, A. V.: 1992, Colloid transport through fractured and unfractured laboratory sand columns, *J. Contam. Hydrol.* **9**, 289–303.

Tsang, Y. W. and Tsang, C. F.: 1987, Channel model of flow through fractured media, *Water Resour. Res.* **23**, 467–479.

van der Lee, J., Ledoux, E. and de Marsily, G.: 1992, Modeling of colloidal uranium transport in a fractured medium, *J. Hydrol.* **139**, 135–158.

Vogler, E. T. and Chrysikopoulos, C. V.: 2001, Dissolution of nonaqueous phase liquid pools in anisotropic aquifers, *Stochastic Environ. Res. Risk Assess.* **15**, 33–46.